



# Probing the intrinsic active sites of modified graphene oxide for aerobic benzylic alcohol oxidation

Shanhui Zhu <sup>a,\*</sup>, Youliang Cen <sup>a,b</sup>, Miao Yang <sup>c</sup>, Jing Guo <sup>a,b</sup>, Chengmeng Chen <sup>a,d</sup>,  
Jianguo Wang <sup>a</sup>, Weibin Fan <sup>a,\*</sup>

<sup>a</sup> State Key Laboratory of Coal Conversion, Institute of Coal Chemistry, Chinese Academy of Sciences, Taiyuan 030001, PR China

<sup>b</sup> University of Chinese Academy of Sciences, Beijing 100039, PR China

<sup>c</sup> Department of Chemistry, University of Wisconsin-Madison, 1101 University Avenue, Madison, WI 53706, United States

<sup>d</sup> Key Laboratory of Carbon Materials, Institute of Coal Chemistry, Chinese Academy of Sciences, Taiyuan 030001, PR China



## ARTICLE INFO

### Article history:

Received 25 December 2016

Received in revised form 7 April 2017

Accepted 10 April 2017

Available online 13 April 2017

### Keywords:

Graphene oxide

Benzylic alcohol

Oxidation

Metal-free

Active sites

## ABSTRACT

The graphene-based materials, particularly graphene oxide (GO) with rich oxygenated groups, exhibit high catalytic performance in various metal-free oxidation reactions. However, the intrinsic active site is still unclear, which greatly retards to further develop advanced catalysts. Here, the modified graphene oxide (abGO) was synthesized by sequential base and acid treatment and employed in the aerobic oxidation of benzyl alcohol to benzaldehyde. This novel catalyst displayed much higher activity, selectivity and stability than that of conventional GO. 93.1% conversion and 100% selectivity were achieved over abGO. More importantly, it is shown that the yield of benzaldehyde is linearly proportional to the content of surface phenol hydroxyl groups. Experimentally observed reactivity trends, structure-behavior correlation, molecule mimicking and characterization results strongly confirm that the surface phenol hydroxyl groups are the intrinsic active sites.

© 2017 Elsevier B.V. All rights reserved.

## 1. Introduction

The selective oxidation of alcohols to aldehydes is fundamentally important both in academic laboratories and industry. These products are valuable fine chemicals and versatile intermediates for perfume, pharmaceuticals, agrochemicals and polymers [1,2]. The conventional oxidation of alcohols is usually performed using toxic stoichiometric reagents, such as chromate or permanganate [2–4]. During the last decade, the heterogeneous metal-based catalysts including Au, Pt and Pd have been extensively employed for aerobic oxidations of alcohols owing to their outstanding catalytic performances under mild conditions. Hutchings et al. [1] showed that Au-Pd/TiO<sub>2</sub> catalyst gave unprecedented high turnover frequency for the oxidation of several kinds of alcohols. Kobayashi et al. [5] developed an efficient polymer incarcerated gold (PI Au) with excellent performance at room temperature in O<sub>2</sub> with the aid of K<sub>2</sub>CO<sub>3</sub>. Tsukuda et al. [6] described the thiolate-mediated selectivity control by hierarchically porous carbon nanosheets supported Au. The other relatively feasible catalysts include Au/Ga<sub>3</sub>Al<sub>2</sub>O<sub>9</sub> [7], Au/CuO [8], Pd/CNS [9], PtBi/CNT [10], Pd@N-doped carbon [11],

Pd/HAP [12], ARP-Pt [13], Pd on graphene [14] and encapsulated Pd in ionic copolymer [15]. Nevertheless, these metal catalysts suffer from expensive cost, limited availability and toxic properties. Therefore, the development of environmental benign and cost-effective procedures for the oxidation of alcohols continues to gain great interest. In this respect, it is highly desirable to devise effective metal-free catalyst and use O<sub>2</sub> as oxidant together with water as solvent. As a result, the nanocarbon-based catalysis has been shown to be potential alternative to meet the requirements of sustainable chemistry [16–19]. Kakimoto et al. [17] reported that nitric acid assisted nanoshell carbon smoothly oxidized benzyl alcohol in 1,4-dioxane and afforded high conversion and good selectivity to aldehydes. However, the use of nitric acid increased the difficulty of product separation and also corroded the reactor. Peng et al. [19] claimed that carbon nanotubes could selectively oxidize benzyl alcohol to benzaldehyde in the absence of nitric acid, but the conversion was only 30.3% even under relatively high temperature (130 °C) and O<sub>2</sub> pressure (1.5 MPa). The nitrogen doping mildly improved the conversion of benzyl alcohol to 44.7%. Interestingly, the authors deduced that the surface carboxylic acid groups were greatly detrimental for the catalytic reactivity while the graphene skeletons played a crucial role in activate O<sub>2</sub>.

Graphene and its derivative graphene oxide (GO) have attracted tremendous attention, and have been widely applied in the field

\* Corresponding authors.

E-mail addresses: [zhushanhui@sxicc.ac.cn](mailto:zhushanhui@sxicc.ac.cn) (S. Zhu), [fanwb@sxicc.ac.cn](mailto:fanwb@sxicc.ac.cn) (W. Fan).

of electronic and photonic devices, catalysis, sensors and energy-storage materials due to their exceptional physical properties and chemical tunability [20–24]. Because of the exhaustive oxidation process in Hummer's method, GO unavoidably possesses several kinds of surface functional groups, such as phenol hydroxyl, carbonyl, and carboxylic acid groups, which provide its moderate acidic and oxidizing properties [25–29]. Dreyer et al. [30] pioneered the use of GO as a metal-free carbon-based catalyst to catalyze the oxidations of various alcohols and hydration of alkynes. Since then, GO or modified materials have been gradually adopted as oxidizing catalysts for the oxidations of amines [31], alcohols [30,32,33], aldehydes [34], benzene [35] and ethylbenzene [36,37]. Porous GO fabricated by Su et al. [36] gave 65% conversion for the oxidative dehydrogenation of ethylbenzene to styrene at 400 °C. They insisted that the unpaired electrons at the edges of defects can activate oxygen molecules and promote the reaction. Liu et al. [33] identified the carboxyl groups as the active sites and the reduced form could be reoxidized by O<sub>2</sub>. Owing to the non-stoichiometric and inhomogeneous nature of GO, the intrinsic active sites are still unclear and controversial, making it impossible to study the detailed reaction mechanism or compare the performance of GO bearing different structures objectively and fairly. The surface carbonyl, carboxylic acid, epoxide groups or even graphene skeletons have been regarded as active sites [30,31,33–36]. Therefore, it is urgent to explore the intrinsic active species in governing the reaction rate and activate O<sub>2</sub>. Additionally, GO usually suffers from low activity and stability in liquid-phase reaction, which greatly limits its wide applications.

In this work, we have presented a facile method to regulate the surface oxygen-containing groups of GO by the sequential treatment of base and acid. The modified GO with enhanced phenol hydroxyl groups greatly improved the activity as well as stability, and showed good substrate adaptability in the oxidation of benzylic alcohols. More importantly, the structure-behavior relationship and intrinsic active sites were well revealed.

## 2. Experimental

### 2.1. Chemicals and reagents

Graphite power (Aladdin), H<sub>2</sub>SO<sub>4</sub> (98 wt.%, Xilong Chem. Co. Ltd, China), NaNO<sub>3</sub> (Kermel Chem. Reagent Co. Ltd, China), KMnO<sub>4</sub> (Kermel Chem. Reagent Co. Ltd, China), H<sub>2</sub>O<sub>2</sub> (30%, Dong Fang Chem. Co. Ltd, China), NaOH (Sinopharm Chemical Reagent Co., Ltd, China (SCRC)), bromoacetic acid (Aladdin), NaBH<sub>4</sub> (SCRC), hydrochloric acid (SCRC), benzyl alcohol (SCRC), 4-methyl and 4-methoxybenzyl alcohols (SCRC), 4-nitrobenzyl alcohol (SCRC), cinnamic alcohol (Shanghai Shuangxiang Reagent Co. Ltd, China), furfuryl alcohol (SCRC), 2-thiophene methanol (Tokyo Chemical Industry Co. Ltd (TCI)), anthraquinone (SCRC), 1-naphthalene carboxylic acid (SCRC), 1-pyrenebutyric acid (SCRC), 1-naphthol (SCRC), guaiacol (SCRC), 4-ethylguaiacol (TCI) and vanillin (SCRC).

### 2.2. Catalyst preparation

GO was synthesized by a modified Hummer's method [25]. 5 g graphite and 2.5 g NaNO<sub>3</sub> were stirred in 115 mL 98 wt.% H<sub>2</sub>SO<sub>4</sub> under ice bath condition. 15 g KMnO<sub>4</sub> was added into the reaction solution and heated to 35 °C under vigorous stirring for 30 min. The system was diluted by 230 mL deionized water, heated to 98 °C, and introduced additional 700 mL water. After adding 50 mL H<sub>2</sub>O<sub>2</sub>, the suspension was filtered, washed and dried at 50 °C. The dispersed graphite oxide in water was processed by sonication for 60 min, centrifugated and dried at ambient temperature.

10 g NaOH and 15 g bromoacetic acid were added into 200 mL GO aqueous solution (1 mg/mL) with vigorous stirring and sonication for 5 h at room temperature. Subsequently, the mixture was neutralized to pH = 7 by adding hydrochloric acid and stirred for 2 h. After dialyzing 72 h by cellulose ester dialysis membranes (molecular weight cut-off 8000–10000, Solarbio corporation), the mixture was rinsed repeatedly, centrifugated, and dried at 80 °C. The as-synthesized sample was denoted as abGO, while the sample was denominated as bGO without the neutralization of hydrochloric acid. The preparation procedures of abGO are illustrated in Scheme S1 in Supporting Information.

1 g NaBH<sub>4</sub> was added to 200 mL abGO aqueous solution (1 mg/mL) under stirring for 3 h. Subsequently, the suspension was neutralized to pH = 7 by adding hydrochloric acid and stirred for 2 h. Subsequently, the mixture was centrifugated, and dried at 80 °C. The obtained material was named as arabGO, while the sample was denoted as rabGO without the neutralization of hydrochloric acid.

### 2.3. Catalyst characterization

N<sub>2</sub> adsorption–desorption isotherms were performed at –196 °C on a Micromeritics TriStar 3000 instrument. Prior to the measurements, the catalysts were evacuated under vacuum at 150 °C for 8 h. The IR spectra were obtained from Vertex 70 (Bruker) FT-IR spectrophotometer in the range of 400–4000 cm<sup>–1</sup> with a resolution of 4 cm<sup>–1</sup>. Raman spectroscopy was exhibited using a Renishaw UV-vis Raman System 1000 with a multichannel air-cooled CCD detector at room temperature. An Nd-Yag laser operating at 532 nm was utilized as the excitation source with a power of 30 MW. The solid-state C<sup>13</sup> NMR spectra were measured on a Bruker Avance spectrometer with MAS spin rate at 9000 Hz. XPS spectra were collected from a Kratos AXIS ULTRA DLD spectrometer with Al K $\alpha$  radiation and a multichannel detector. The binding energy was calibrated by C 1s peak at 284.6 eV with  $\pm 0.1$  eV error. Transmission electron microscopy (TEM) and high-resolution transmission electron microscopy (HRTEM) measurements were performed in JEM 2011F apparatus operating at 200 kV voltages. The samples were dispersed in ethanol under ultrasonic conditions for 30 min and then deposited on carbon-coated copper grids.

### 2.4. Catalytic tests

The reactions were performed in a Teflon-lined stainless steel autoclave containing 0.25 mmol feed, 10 mL water and 0.05 g catalyst. The reactor was purged by flushing O<sub>2</sub> with five times, and maintained at 100 °C and 0.2 MPa O<sub>2</sub> for designated time. When the reaction was terminated, the reactor system was quickly cooled to room temperature in an ice-water bath. The solid catalyst was separated by repeatedly centrifugation and then dried at 80 °C. The spent catalyst was conducted for reusability test under the same conditions as above. The liquid mixture was extracted with ethyl acetate, and ethyl benzoate was used as internal standard. The products were analyzed by gas chromatography (Shimadzu GC-2010) using a flame ionization detector with a DB-1 capillary column (60 m × 0.25 mm × 0.25  $\mu$ m). The C-mass balance was estimated in the range of ca. 97%–101%. All the products were identified by GC-MS.

## 3. Results and discussion

### 3.1. Catalyst characterization

TEM and HRTEM images of GO and modified samples are illustrated in Fig. 1. All the samples displayed typical nanosheet structure of graphene with ca. 2–10 layers. Compared to GO, the

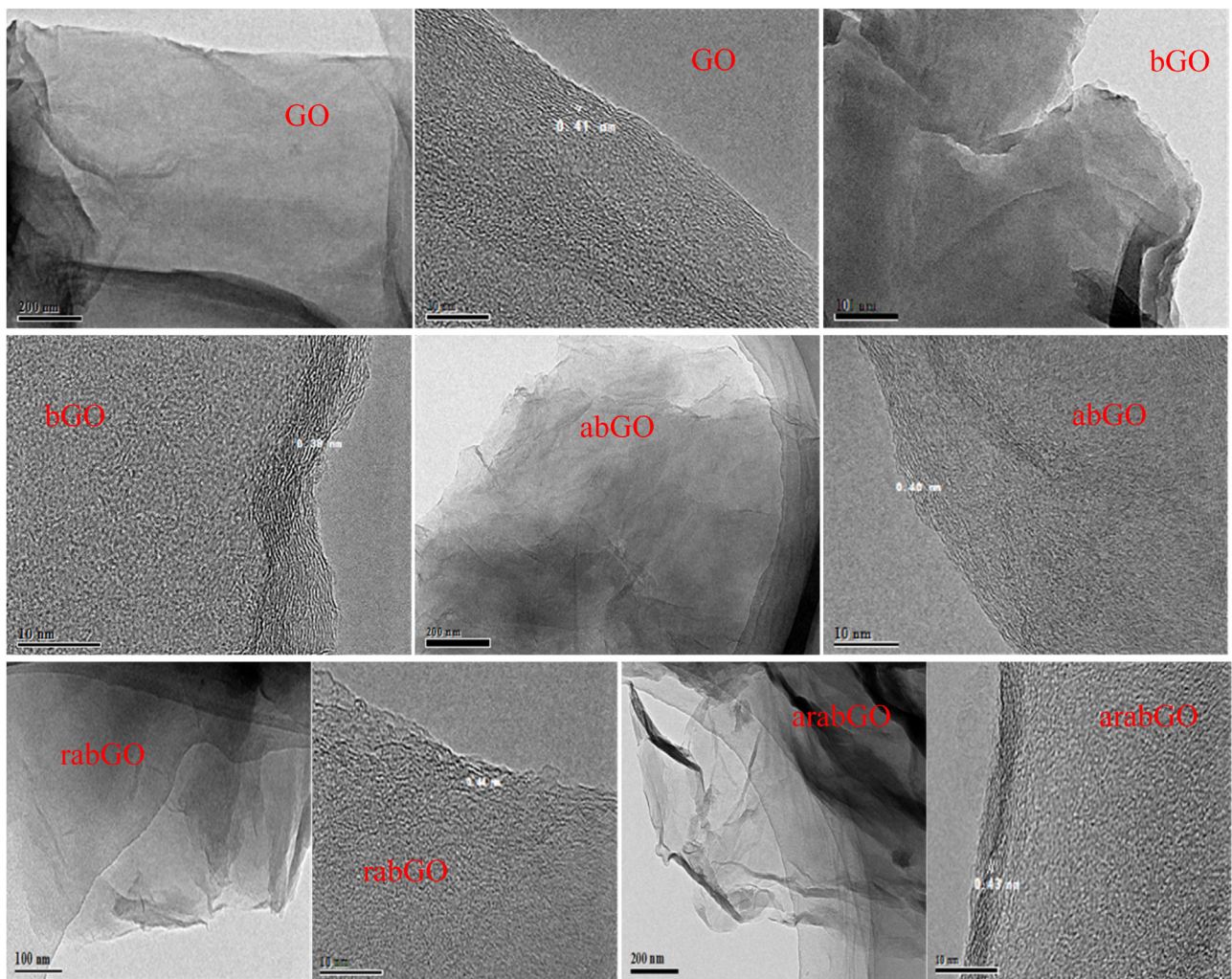


**Fig. 1.** TEM and HRTEM images of GO and modified catalysts.

modified samples showed less layers of graphene nanosheets, particularly for  $\text{NaBH}_4$  reduced rabGO and arabGO. Notably, some defects and crumpled structure were observed, which mainly resulted from the severe oxidation process. The treatment by base and acid only increased a few defects, but did not cause significant damage on the nanosheet structure. The interlayer spacing is averagely *ca.* 0.40 nm, and larger than that of graphite (0.34 nm) owing to the presence of oxygenated groups [38,39].

As listed in Table 1, the BET surface area of GO increased obviously after its treatment by base and acid, because the vigorous sonication facilitated the exfoliation of GO nanosheets and the modification promoted the elimination of partial oxygenated groups. The processing by  $\text{NaBH}_4$  further improved BET surface area, for it showed strong reduction ability on oxygenated groups of interlamellar spaces between adjacent graphene layers. The elimination of oxygenated groups favorably exfoliated graphene layers, and thus declined its layer number.

As shown in Fig. 2 of Raman spectroscopy, all the samples exhibited two distinct peaks centered at  $1335$  and  $1597\text{ cm}^{-1}$ , which were assigned to D and G band, respectively [32,34]. The D band is indicative of the defects such as disorders, edges and boundaries, while the G band is a signature for the existence of  $\text{sp}^2$ -hybridized carbon atoms of graphene [40]. The intensity ratio of  $I_D/I_G$  is used to reflect the density of defects. The value of  $I_D/I_G$  increased slightly after GO was treated by base and acid. Compared to GO, the ratio improved from 1.15 to 1.28 over rabGO, suggesting that more struc-

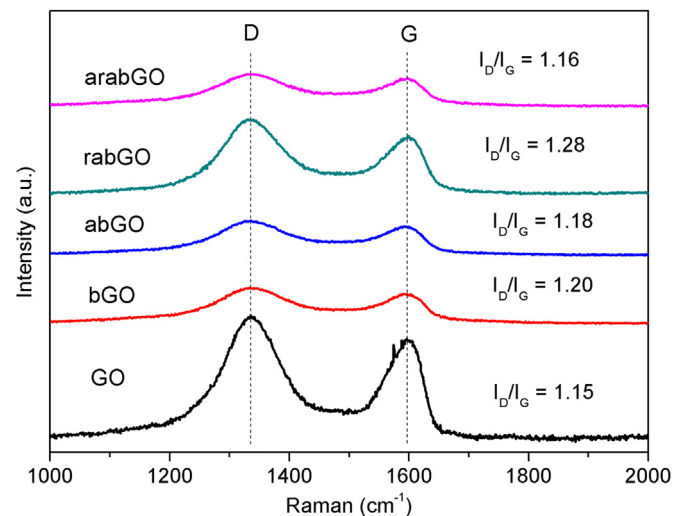


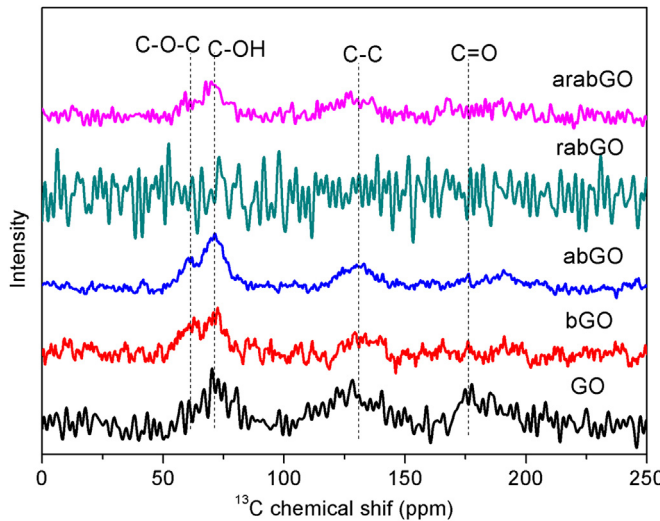
**Fig. 2.** Raman spectra of GO and modified catalysts.

tural defects were created by the reduction of  $\text{NaBH}_4$ . Notably, the absolute intensity of Raman spectra depends on the film thickness, *e.g.* the number of graphene layers [41]. Therefore, the low intensity of modified GO reflected the reduced graphene layers and enhanced quality, consistent well with the results from TEM.

**Table 1**

BET surface area, XPS O1s data and the ratio of C/O.

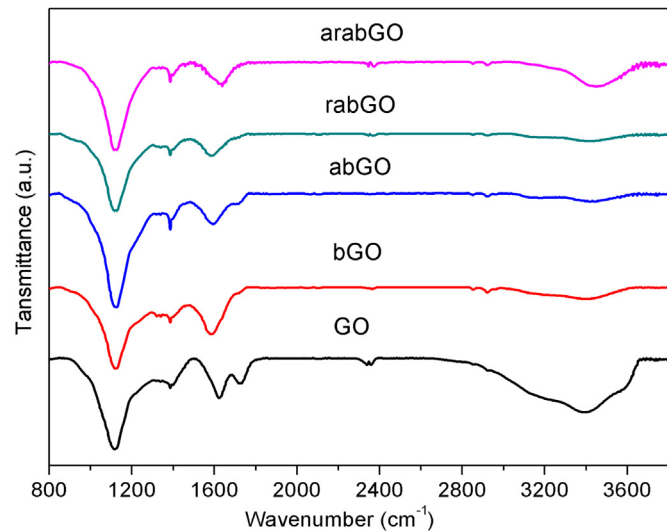
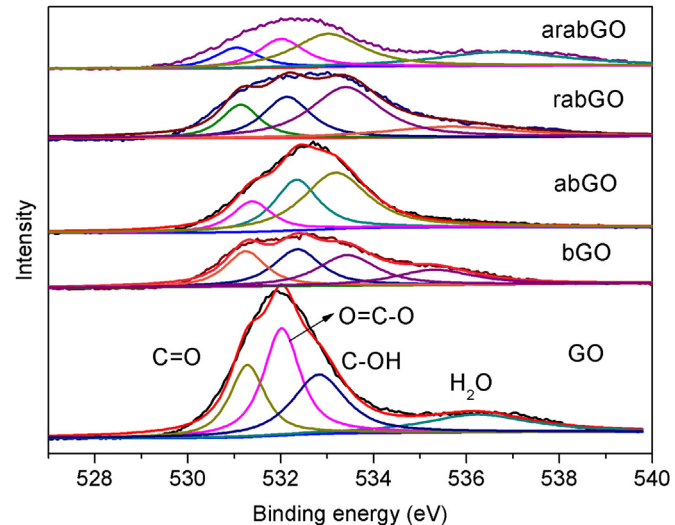
Catalyst	$S_{\text{BET}}$ ( $\text{m}^2/\text{g}$ )	C/O	C=O (at.%)	$\text{O}=\text{C}-\text{O}$ (at.%)	C—OH (at.%)
GO	41.2	1.8	7.33	10.30	8.18
bGO	75.6	2.6	6.85	7.82	6.63
abGO	84.5	3.2	6.35	6.75	10.60
rabGO	132.2	3.5	4.04	5.44	6.57
arabGO	139.7	3.4	3.50	4.00	9.35

**Fig. 3.**  $^{13}\text{C}$  NMR spectra of GO and modified catalysts.

$^{13}\text{C}$  NMR spectra were employed to identify various functional groups and the results are illustrated in Fig. 3. GO showed a broad peak at 71 ppm as well as a weak should peak at 61 ppm, which were assigned to the phenol hydroxyl and epoxide groups, respectively [31]. Compared to GO, the sequential NaOH and HCl treatment of abGO increased the quantities of phenol hydroxyl groups. This was mostly probably due to the addition of bromoacetic acid, which was favorable to convert epoxides into hydroxyl groups, and the HCl treatment also facilitated to recover them [42]. However, the peak of C=O groups at 176 ppm remarkably decreased [43], revealing that many carbonyl or carboxyl groups were removed via the processing of based and acid. The broad peak at 131 ppm suggested that the  $\text{sp}^2$  conjugation C=C of graphene was largely reserved with the loss of oxygenated groups.

FTIR spectra of all the fresh samples are illustrated Fig. 4. A broad peak at 3000–3600  $\text{cm}^{-1}$  was observed over GO, which was mainly assigned to hydroxyl groups of strongly adsorbed  $\text{H}_2\text{O}$ , phenol hydroxyl and carboxyl groups [31]. After the treatment of base and acid, this peak significantly decreased due to the removal of much water. Similarly, the peaks of carboxyl and carbonyl groups centered at 1730 and 1620  $\text{cm}^{-1}$  remarkably decreased over modified GO [25]. The peak at 1580  $\text{cm}^{-1}$  became strong after the base treatment, which was associated with the  $\text{sp}^2$ -hybdridized C=C [31]. Subsequently, the acid and  $\text{NaBH}_4$  processing decreased the intensity of C=C. The peak at 1380  $\text{cm}^{-1}$  was corresponding to epoxides [28]. GO showed a strong peak at 1110  $\text{cm}^{-1}$ , which was attributed to the phenol hydroxyl group [31]. Its intensity was decreased after base treatment, while recovered and even obviously increased by subsequent acid processing. The  $\text{NaBH}_4$  reduction significantly dropped the phenol hydroxyl group while the final acid treatment largely recovered it again.

As shown in Fig. 5, the peak area through the deconvolution of O 1s XPS spectra provides information on the relative surface concentration of various O species, and the corresponding results as well as the ratio of C/O are summarized in Table 1. The decon-

**Fig. 4.** FTIR spectra of GO and modified catalysts.**Fig. 5.** O 1s XPS spectra of GO and modified catalysts.

voluted four peaks at *ca.* 531.4, 532.6, 533.4 and 536.1 eV were classified into carbonyl, carboxyl, phenol hydroxyl and adsorbed  $\text{H}_2\text{O}$  groups, respectively [44–46]. Compared to GO, the surface concentrations of carbonyl and carboxyl groups obviously decreased through the treatment of base and acid, consistent with the NMR and FTIR results. The increase of C/O ratio also confirmed the elimination of partial oxygenated groups. The base treatment dropped the amounts of phenol hydroxyl groups, while they were recovered and increased through further neutralization by acid. Similarly, the  $\text{NaBH}_4$  processing of abGO declined the phenol hydroxyl groups from 10.60% to 6.57%. Also, these groups were recovered to 9.35% by acid treatment.  $\text{NaBH}_4$  plays important role in dehydroxylation, while hydrochloric acid can catalyze the ring-opening of epoxy

**Table 2**

Oxidation of benzyl alcohol to benzaldehyde over various graphene-based catalysts.<sup>a</sup>

Entry	Catalyst	Conversion (%)	Selectivity (%)
1	GO	45.7	94.7
2	bGO	26.9	100
3	abGO	76.5	100
4	rabGO	26.8	100
5	arabGO	68.5	100

<sup>a</sup> Reaction conditions: 0.05 g catalyst, 0.25 mmol benzyl alcohol, 10 mL H<sub>2</sub>O, 100 °C, 0.2 MPa O<sub>2</sub>, 24 h.

groups to generate hydroxyl groups [38]. Meanwhile, NaBH<sub>4</sub> is rather effective in reducing carbonyl groups but has moderate efficiency in the reduction of carboxylic acid species.

Based on above characterization results, it can be seen that the modified GO improved the quality of graphene nanosheets. Moreover, the surface defects mildly increased upon the treatment of base and acid. More importantly, this method can be employed to control the surface oxygen-containing groups of GO. e.g. The abGO catalyst substantially removed the carbonyl and carboxyl groups while improved the phenol hydroxyl groups contents.

### 3.2. Catalytic performance of benzylic alcohol oxidation

Fig. S1 displays the effect of reaction parameters on the catalytic performance of aerobic oxidation of benzyl alcohol to benzaldehyde over abGO. The evaluation of various metal-free catalysts was investigated in water under optimized conditions at 100 °C and 0.2 MPa O<sub>2</sub> for 24 h. As described in Table 2, GO gave 45.7% conversion of benzyl alcohol and 94.7% selectivity to benzaldehyde. The other by-product was benzoic acid due to deep oxidation. However, the conversion declined from 45.7% to 26.9% after GO was treated by base. Interestingly, the consecutive acid-treated GO (abGO) exhibited remarkably enhanced catalytic activity and the conversion reached 76.5%. When abGO was processed by NaBH<sub>4</sub>, the reactivity substantially declined and the conversion was only 26.8%. The conversion was largely recovered again after rabGO was neutralized by hydrochloric acid. It should be noted that all the modified catalysts presented enhanced benzaldehyde selectivity and reached 100%, which may result from the removal of unstable and particularly reactive oxygenated groups. Of them, the abGO catalyst showed the best catalytic performance in this study.

As reported previously [25,47,48], graphene-based materials are usually unstable upon reusability test owing to the loss of oxygenated groups. Fig. 6 displays the catalytic behavior of reusability tests for GO and abGO. Evidently, GO presented serious deactivation upon five reaction cycles. Specifically, the conversion of benzyl alcohol distinctly decreased from 45.7% to 20.9% of the fifth run. Unexpectedly, the conversion of benzyl alcohol did not decline even upon eight times tests over abGO. This demonstrates its excellent stability upon 192 h long-term test. The robust structure of abGO is strongly related to the removal unstable oxygenated groups by base and acid treatment. Above all, the abGO catalyst is an active, selective and stable catalyst under green conditions, which is superior to previous metal-free counterparts (Table S1) [17–19,30,32].

Moreover, abGO was active and selective for the aerobic oxidation of various benzylic and aromatic alcohols, an indication of its great versatility. As shown in Table 3, the conversion of benzyl alcohol was further improved to 93.1% when the reaction time was prolonged to 30 h. Good conversions and selectivities were achieved in the conversion of substituted benzyl alcohols. Generally, the substrates with electron-donating groups such as 4-methyl and 4-methoxy benzyl alcohols exhibited superior activity. Conversely, moderate conversion of electron-withdrawing 4-nitrobenzyl alcohol was obtained with 81.7%. Regarding cin-

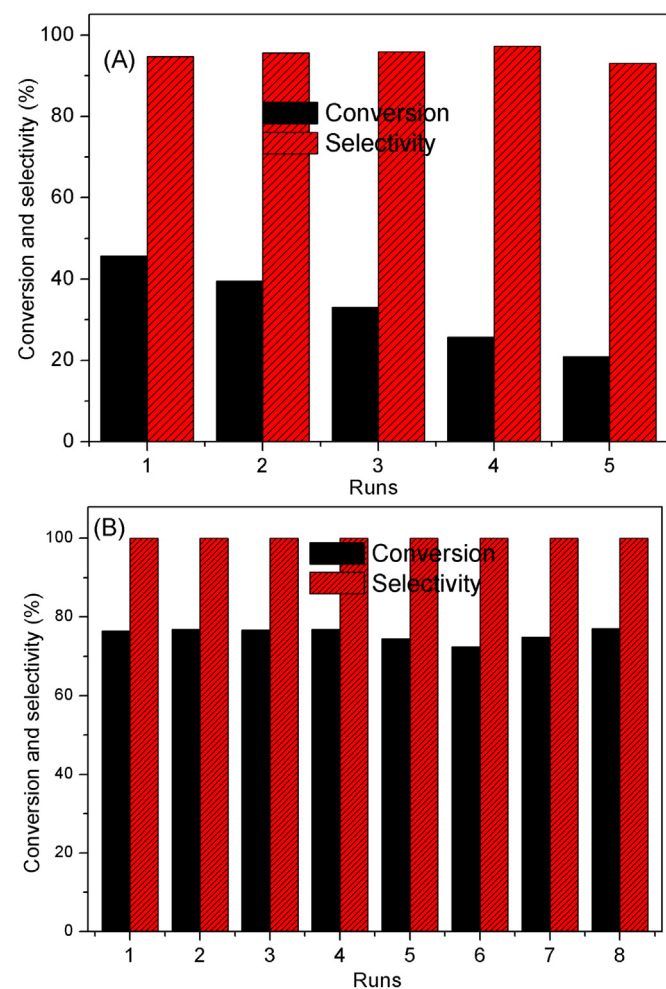


Fig. 6. The reusability tests of (A) GO and (B) abGO for benzyl alcohol oxidation to benzaldehyde. Reaction conditions: 0.05 g abGO, 0.25 mmol benzyl alcohol, 10 mL H<sub>2</sub>O, 100 °C, 0.2 MPa O<sub>2</sub>, 24 h.

namic alcohol, high yields of partial oxidized cinnamic aldehyde was achieved. Oxidation of furfuryl alcohol, a substrate that is abundantly available from biomass and of interest for biomass utilization [49,50], produced furfural in good conversion and selectivity. 2-thiophene methanol could be smoothly oxidized to obtain the corresponding aldehyde in good yields over abGO. As for secondary alcohol, abGO was also active for the oxidation of 1-phenyl ethanol with 75.1% conversion and 95.2% selectivity to acetophenone.

### 3.3. Probe the intrinsic active sites

Owing to the non-stoichiometric and inhomogeneous nature, graphene skeletons, defects sites, carbonyl, or carboxylic groups have been identified as the active centers in previous reports [27,30,31,34,36]. To understand the reaction mechanism, it is essential and interesting to explore the intrinsic active species. Compared to GO, the modified rabGO and bGO displayed good and few graphene layers, but presented lower reactivity, indicating that the graphene skeletons should not be the active species. As can be seen from Tables 1 and 2, there is no direct correlation between BET surface area and catalytic activity, reflecting that the textural properties did not control the reaction. In addition, rabGO and bGO showed high I<sub>D</sub>/I<sub>G</sub> and possessed many defects sites, but their bad performance confirmed that the defects sites did not play crit-

**Table 3**Oxidation of various aromatic alcohols into corresponding aldehydes over abGO.<sup>a</sup>

Entry	Substrate	Product	Conversion (%)	Selectivity (%)
1			93.1	100
2			96.8	100
3			100	99.7
4			81.7	98.5
5			89.5	99.5
6			100	85.6
7			100	98.7
8			75.1	95.2

<sup>a</sup> Reaction conditions: 0.05 g abGO, 0.25 mmol aromatic alcohol, 10 mL H<sub>2</sub>O, 100 °C, 0.2 MPa O<sub>2</sub>, 30 h.

ical role in governing the reaction. Thereby, the active centers are mostly related to the oxygen-containing groups.

Subsequently, a series of model molecules including anthraquinone, 1-naphthalenecarboxylic acid, 1-pyrenebutyric acid, 1-naphthol, guaiacol, 4-ethylguaiacol and vanillin could be used as model catalysts to mimic the roles of carbonyl, carboxyl and phenol hydroxyl groups in the aerobic oxidation of benzyl alcohol. As listed in Table 4, the blank experiment showed that the conversion of benzyl alcohol was 3.8% at 100 °C and 0.2 MPa O<sub>2</sub> for 24 h. Anthraquinone, 1-naphthalenecarboxylic acid and 1-pyrenebutyric acid were not active relative to the blank test, suggesting that the carbonyl and carboxyl groups could not be the active species. Unexpectedly, the use of 1-naphthol, guaiacol and 4-ethylguaiacol were effective for the oxidation of benzyl alcohol. Guaiacol exhibited the best performance and the conversion of benzyl alcohol reached 27.3%. These results imply that phenol hydroxyl group plays an important role and may be the active species. Additionally, the conversion decreased to 5.4% over vanillin, because the aldehyde group was probably detrimental for the reaction.

It is clearly observed that phenol hydroxyl group favors aerobic oxidation of benzyl alcohol to benzaldehyde. As displayed in Tables 1 and 2, it seems that the conversion of benzyl alcohol is roughly proportional to the concentration of phenol hydroxyl group, while the selectivity to benzaldehyde is ≥94.7% in all the catalysts. Thus, we attempt to correlate the concentration of phenol hydroxyl group with the yield of benzaldehyde, and the result is illustrated in Fig. 7. Interestingly, a precisely linear relationship is obtained, revealing the essential active sites of phenol hydroxyl group for the selective oxidation of benzyl alcohol to benzaldehyde.

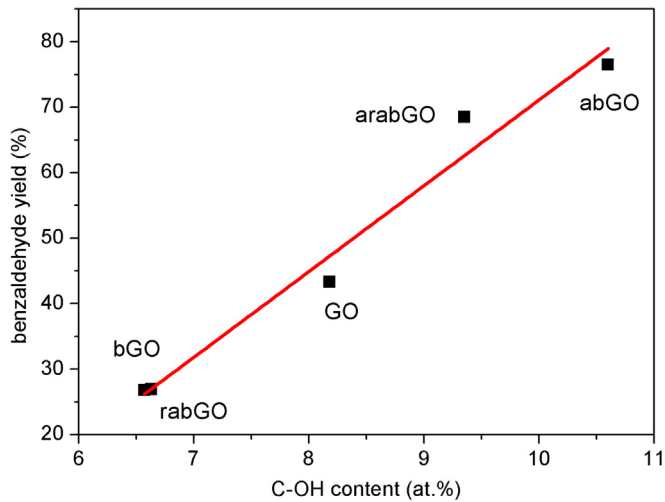


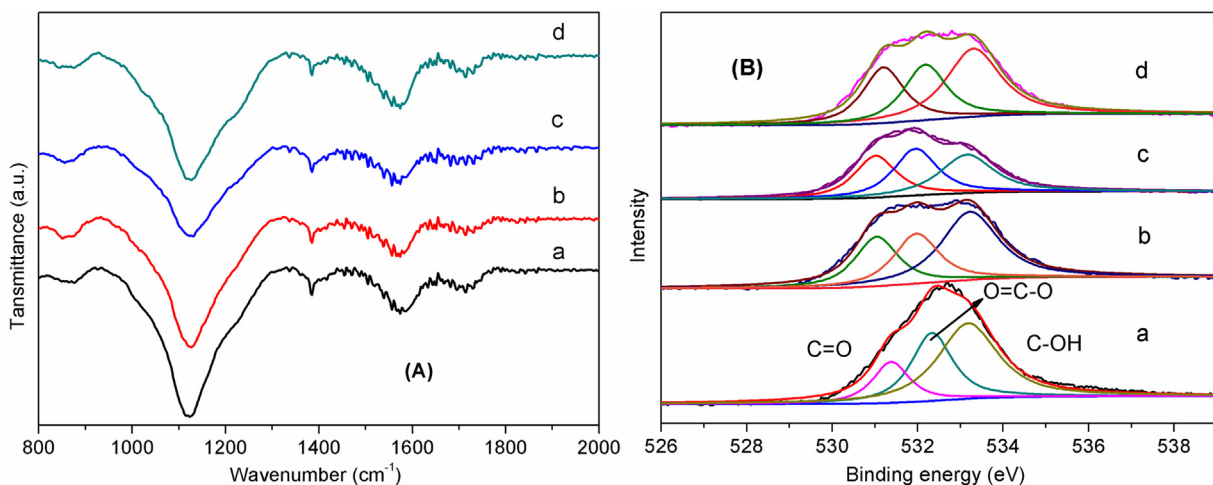
**Fig. 7.** Correlation between the content of phenol hydroxyl groups and benzaldehyde yield. Reaction conditions: 0.05 g abGO, 0.25 mmol benzyl alcohol, 10 mL H<sub>2</sub>O, 100 °C, 0.2 MPa O<sub>2</sub>, 24 h.

Obviously, the excellent performance of abGO is attributed to the substantial amounts of phenol hydroxyl groups.

As mentioned previously [51,52], the phenolic compounds have dual roles as antioxidants or oxidants during plant growth, metabolism and even physiological activity in human. At relatively low concentrations, they are susceptible to be oxidized to quinones by O<sub>2</sub> or free radical, which makes them behave as antioxidants. At

**Table 4**Oxidation of benzyl alcohol to benzaldehyde over various model molecules.<sup>a</sup>

Entry	Model chemicals	Catalyst name	Conversion	Selectivity
			(%)	(%)
1	blank	-	3.8	100
2		anthraquinone	4.7	100
3		1-naphthalenecarboxylic acid	4.0	100
4		1-pyrenebutyric acid	4.6	100
5		1-naphthol	17.3	100
6		guaiacol	27.3	100
7		4-ethylguaiacol	17.8	100
8		vanillin	5.4	100

<sup>a</sup> Reaction conditions: 0.05 g catalyst, 0.25 mmol benzyl alcohol, 10 mL H<sub>2</sub>O, 100 °C, 0.2 MPa O<sub>2</sub>, 24 h.**Fig. 8.** FTIR (A) and XPS (B) spectra of (a) fresh abGO; (b) abGO (0.05 g) was treated by 0.25 mmol benzyl alcohol in 10 mL water at 100 °C and 0.2 MPa N<sub>2</sub> for 24 h; (c) abGO (0.05 g) was treated by 0.2 MPa O<sub>2</sub> in 10 mL water at 100 °C for 24 h; (d) abGO (0.05 g) was co-treated by 0.25 mmol benzyl alcohol and 0.2 MPa O<sub>2</sub> in 10 mL water at 100 °C for 24 h.

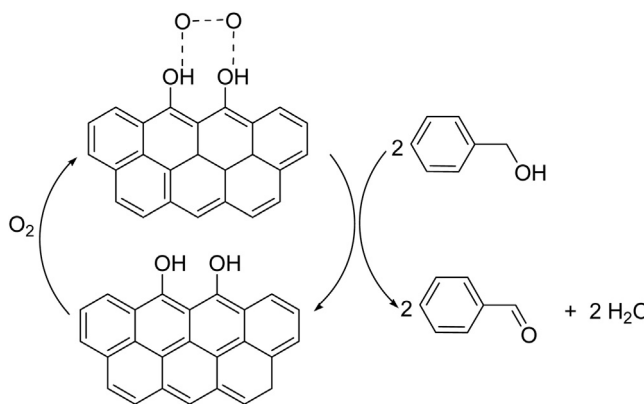


**Fig. 9.** Proposed reaction mechanism for the aerobic oxidation of benzyl alcohol to benzaldehyde over abGO.

higher concentrations, they are functional as oxidants due to their involvement in initiation reactions. It is reported that the phenolic compounds are capable of forming complexes with  $\text{Cu}^0$  or  $\text{Fe}^0$  and finally oxidize them to polyvalent cations [51]. To deeply explore the roles of phenol hydroxyl group during the aerobic oxidation of benzyl alcohol, FTIR and XPS spectra of abGO with different treatments were investigated and the results are displayed in Fig. 8. The concentrations of functional groups are listed in Table S2. Compared to fresh abGO, no distinct change was observed after it was processed with benzyl alcohol alone. However, the peak of phenol hydroxyl group at  $1110\text{ cm}^{-1}$  declined remarkably and the XPS result definitely showed its sharp decrease when abGO was treated by  $\text{O}_2$ . This strongly reveals that phenol hydroxyl group can adsorb and activate  $\text{O}_2$ . Finally, the concentration of phenol hydroxyl group was mostly preserved over spent abGO in the co-treatment of benzyl alcohol and  $\text{O}_2$ , since the activated  $\text{O}_2$  could smoothly oxidize benzyl alcohol and the phenol hydroxyl group was recovered again. The excellent stability of abGO also reflects its good catalytic cycle. In sum, the above results undoubtedly verify that the phenol hydroxyl group should be the intrinsic active species. Based on above discussions, the proposed reaction mechanism for the aerobic oxidation of benzyl alcohol to benzaldehyde over abGO is illustrated in Fig. 9. According to Eley-Rideal mechanism, the phenol hydroxyl groups adsorb and activate molecular oxygen. Subsequently, the activated  $\text{O}_2$  can directly attack the  $\alpha$ -H atom of benzyl alcohol to form benzaldehyde and release  $\text{H}_2\text{O}$ .

#### 4. Conclusions

This work has developed a facile method involving consecutive base and acid treatment for the synthesis of modified GO, which removes the unstable oxygenated species and improves the content of phenol hydroxyl groups. The novel material abGO exhibited superior conversion of benzyl alcohol and 100% selectivity to benzaldehyde. This catalyst was rather robust and did not suffer from deactivation in eight consecutive reaction cycles. The amount of surface phenol hydroxyl groups is linearly increased with the yield of benzaldehyde, giving direct evidence that phenol hydroxyl groups are the intrinsic active species. The molecule mimicking and characterization results also strongly reveal that the phenol hydroxyl groups can adsorb as well as activate  $\text{O}_2$ , and should play a vital role in catalyze the reaction. The abGO shows extensive substrate adaptability and will hold great potential for wide applications.

#### Acknowledgements

This work was financially supported by National Natural Science Foundation of China (21403269), Natural Science Foundation of Shanxi Province (2016021033), Science Foundation for Youth Scholars of State Key Laboratory of Coal Conversion (2016BWZ002), and Youth Innovation Promotion Association CAS (2015140).

#### Appendix A. Supplementary data

Supplementary data associated with this article can be found, in the online version, at <http://dx.doi.org/10.1016/j.apcatb.2017.04.035>.

#### References

- [1] D.I. Enache, J.K. Edwards, P. Landon, B. Solsona-Espriu, A.F. Carley, A.A. Herzing, M. Watanabe, C.J. Kiely, D.W. Knight, G.J. Hutchings, *Science* 311 (2006) 362–365.
- [2] F. Arena, B. Gumina, C. Cannilla, L. Spadaro, A. Patti, L. Spiccia, *Appl. Catal. B: Environ.* 170–171 (2015) 233–240.
- [3] G. Chen, S. Wu, H. Liu, H. Jiang, Y. Li, *Green Chem.* 15 (2013) 230–235.
- [4] F. Arena, B. Gumina, A.F. Lombardo, C. Espro, A. Patti, L. Spadaro, L. Spiccia, *Appl. Catal. B: Environ.* 162 (2015) 260–267.
- [5] H. Miyamura, R. Matsubara, Y. Miyazaki, S. Kobayashi, *Angew. Chem.* 119 (2007) 4229–4232.
- [6] T. Yoskamtoorn, S. Yamazoe, R. Takahata, J. Nishigaki, A. Thivasathit, J. Limtrakul, T. Tsukuda, *ACS Catal.* 4 (2014) 3696–3700.
- [7] F.-Z. Su, Y.-M. Liu, L.-C. Wang, Y. Cao, H.-Y. He, K.-N. Fan, *Angew. Chem. Int. Ed.* 47 (2008) 334–337.
- [8] H. Wang, W. Fan, Y. He, J. Wang, J.N. Kondo, T. Tatsumi, *J. Catal.* 299 (2013).
- [9] Y. Yan, Y. Dai, S. Wang, X. Jia, H. Yu, Y. Yang, *Appl. Catal.: Environ.* 184 (2016) 104–118.
- [10] C. Zhou, Z. Guo, Y. Dai, X. Jia, H. Yu, Y. Yang, *Appl. Catal.: Environ.* 181 (2016) 118–126.
- [11] P. Zhang, Y. Gong, H. Li, Z. Chen, Y. Wang, *Nat. Commun.* 4 (2013) 1593–1603.
- [12] K. Mori, T. Hara, T. Mizugaki, K. Ebitani, K. Kaneda, *J. Am. Chem. Soc.* 126 (2004) 10657–10666.
- [13] Y.M.A. Yamada, T. Arakawa, H. Hocke, Y. Uozumi, *Angew. Chem.* 119 (2007) 718–720.
- [14] G. Wu, X. Wang, N. Guan, L. Li, *Appl. Catal. B: Environ.* 136–137 (2013) 177–185.
- [15] Q. Wang, X. Cai, Y. Liu, J. Xie, Y. Zhou, J. Wang, *Appl. Catal. B: Environ.* 189 (2016) 242–251.
- [16] H. Watanabe, S. Asano, S. Fujita, H. Yoshida, M. Arai, *ACS Catal.* 5 (2015) 2886–2894.
- [17] Y. Kuang, N.M. Islam, Y. Nabae, T. Hayakawa, M. Kakimoto, *Angew. Chem. Int. Ed.* 49 (2010) 436–440.
- [18] J. Luo, F. Peng, H. Yu, H. Wang, *Chem. Eng. J.* 204–206 (2012) 98–106.
- [19] J. Luo, H. Yu, H. Wang, H. Wang, F. Peng, *J. Chem. Eng.* 240 (2014) 434–442.
- [20] C. Su, K.P. Loh, *Acc. Chem. Res.* 46 (2012) 2275–2285.
- [21] X.-K. Kong, C.-L. Chen, Q.-W. Chen, *Chem. Soc. Rev.* 43 (2014) 2841–2857.
- [22] C. Huang, C. Li, G. Shi, *Energy Environ. Sci.* 5 (2012) 8848–8868.
- [23] S. Zhu, J. Wang, W. Fan, *Catal. Sci. Technol.* 5 (2015) 3845–3858.
- [24] S. Navalón, A. Dhakshinamoorthy, M. Alvaro, H. García, *Chem. Rev.* 114 (2014) 6179–6212.
- [25] S. Zhu, C. Chen, Y. Xue, J. Wu, J. Wang, W. Fan, *ChemCatChem* 6 (2014) 3080–3083.
- [26] A. Dhakshinamoorthy, M. Alvaro, P. Concepcion, V. Fornes, H. García, *Chem. Commun.* 48 (2012) 5443–5445.
- [27] A. Primo, M. Puche, O.D. Pavel, B. Cojocaru, A. Tirsoaga, V. Parvulescu, H. García, *Chem. Commun.* 52 (2016) 1839–1842.
- [28] H. Wang, T. Deng, Y. Wang, X. Cui, Y. Qi, X. Mu, X. Hou, Y. Zhu, *Green Chem.* 15 (2013) 2379–2383.
- [29] X. Gao, S. Zhu, Y. Li, *Catal. Commun.* 62 (2015) 48–51.
- [30] D.R. Dreyer, H.-P. Jia, C.W. Bielawski, *Angew. Chem.* 122 (2010) 6965–6968.
- [31] C. Su, M. Acik, K. Takai, J. Lu, S.-J. Hao, Y. Zheng, P. Wu, Q. Bao, T. Enoki, Y.J. Chabal, K. Ping Loh, *Nat. Commun.* 3 (2012) 1298–1306.
- [32] J. Long, X. Xie, J. Xu, Q. Gu, L. Chen, X. Wang, *ACS Catal.* 2 (2012) 622–631.
- [33] L. Geng, S. Wu, Y. Zou, M. Jia, W. Zhang, W. Yan, G. Liu, *J. Colloid Interface Sci.* 421 (2014) 71–77.
- [34] G. Lv, H. Wang, Y. Yang, T. Deng, C. Chen, Y. Zhu, X. Hou, *ACS Catal.* 5 (2015) 5636–5646.
- [35] J.-H. Yang, G. Sun, Y. Gao, H. Zhao, P. Tang, J. Tan, A.-H. Lu, D. Ma, *Energy Environ. Sci.* 6 (2013) 793–798.
- [36] J. Diao, H. Liu, J. Wang, Z. Feng, T. Chen, C. Miao, W. Yang, D.S. Su, *Chem. Commun.* 51 (2015) 3423–3425.
- [37] Y. Gao, G. Hu, J. Zhong, Z. Shi, Y. Zhu, D.S. Su, J. Wang, X. Bao, D. Ma, *Angew. Chem. Int. Ed.* 52 (2013) 2109–2113.
- [38] S. Pei, H.-M. Cheng, *Carbon* 50 (2012) 3210–3228.

[39] H.-J. Shin, K.K. Kim, A. Benayad, S.-M. Yoon, H.K. Park, I.-S. Jung, M.H. Jin, H.-K. Jeong, J.M. Kim, J.-Y. Choi, Y.H. Lee, *Adv. Funct. Mater.* 19 (2009) 1987–1992.

[40] B. Zhang, J. Song, G. Yang, B. Han, *Chem. Sci.* 5 (2014) 4656–4660.

[41] A. Primo, P. Atienzar, E. Sanchez, J.M. Delgado, H. Garcia, *Chem. Commun.* 48 (2012) 9254–9256.

[42] X. Sun, Z. Liu, K. Welsher, J. Robinson, A. Goodwin, S. Zaric, H. Dai, *Nano Res.* 1 (2008) 203–212.

[43] H.R. Thomas, S.P. Day, W.E. Woodruff, C. Vallés, R.J. Young, I.A. Kinloch, G.W. Morley, J.V. Hanna, N.R. Wilson, J.P. Rourke, *Chem. Mater.* 25 (2013) 3580–3588.

[44] W. Qi, W. Liu, B. Zhang, X. Gu, X. Guo, D. Su, *Angew. Chem. Int. Ed.* 52 (2013) 14224–14228.

[45] G. Wen, S. Wu, B. Li, C. Dai, D.S. Su, *Angew. Chem. Int. Ed.* 54 (2015) 4105–4109.

[46] S. Wu, G. Wen, J. Wang, J. Rong, B. Zong, R. Schlogl, D.S. Su, *Catal. Sci. Technol.* 4 (2014) 4183–4187.

[47] X. Zhao, J. Wang, C. Chen, Y. Huang, A. Wang, T. Zhang, *Chem. Commun.* 50 (2014) 3439–3442.

[48] X. Yu, Y. Huo, J. Yang, S. Chang, Y. Ma, W. Huang, *Appl. Surf. Sci.* 280 (2013) 450–455.

[49] A.C. Alba-Rubio, J.L.G. Fierro, L. León-Reina, R. Mariscal, J.A. Dumesic, M. López Granados, *Appl. Catal. B: Environ.* 202 (2017) 269–280.

[50] S.J. Canhaci, R.F. Perez, L.E.P. Borges, M.A. Fraga, *Appl. Catal. B: Environ.* 207 (2017) 279–285.

[51] K. Robards, P.D. Prenzler, G. Tucker, P. Swatsitang, W. Glover, *Food Chem.* 66 (1999) 401–436.

[52] N. Balasundram, K. Sundram, S. Samman, *Food Chem.* 99 (2006) 191–203.